CrossMark

Fluxing induced boron alloying in Fe-based bulk metallic glasses

Weiming Yang[a], Chao Wan[a], Haishun Liu[a,*], Qiang Li[b], Qianqian Wang[c], Hui Li[d], Jing Zhou[c], Lin Xue[c], Baolong Shen[c,*], Akihisa Inoue[e]

[a] State Key Laboratory for Geomechanics and Deep Underground Engineering, School of Mechanics and Civil Engineering, Institute of Massive Amorphous Metal Science, China University of Mining and Technology, Xuzhou 221116, People's Republic of China
[b] School of Physics Science and Technology, Xinjiang University, Urumqi, Xinjiang 830046, People's Republic of China
[c] School of Materials Science and Engineering, Southeast University, Nanjing 211189, People's Republic of China
[d] School of Materials Science and Engineering, Shanghai University, Shanghai 200444, People's Republic of China
[e] International Institute of Green Materials, Josai International University, Togane 283-8555, Japan

ARTICLE INFO

ABSTRACT

In this work, we report on advanced insights into the effects of fluxing on $Fe_{50}Ni_{30}P_{13}C_7$ bulk metallic glasses. We find that the employed oxide fluxing agent results in significant incorporation of boron in the alloy by atom probe tomography analysis. It demonstrates that the improved glass-forming ability induced by fluxing attributes to not only the reduction of heterogeneous nucleation, but also boron alloying. In addition, the more densely packed microstructure of the fluxed alloys is also related to amount of boron addition. Such an understanding is of great importance to adequately process glass-forming liquids, in order to achieve optimized bulk metallic glass parts with enhanced thicknesses and improved mechanical properties.

GRAPHICAL ABSTRACT
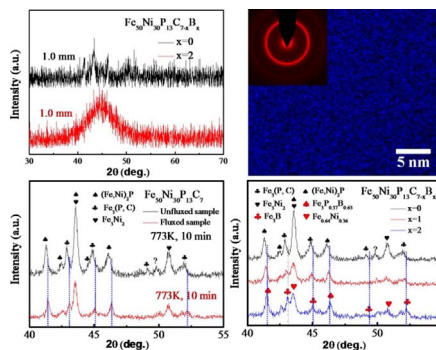
1. Introduction

Fe-based bulk metallic glasses (BMGs) have been investigated for potential uses in electrical transformers, motors, high frequency switching power supplies, and other electrical energy conversion devices [1–5]. However, the commercialization of Fe-based BMGs has been mainly limited by two factors: low critical thickness and high brittleness

[6–10]. There is no doubt that the essential challenge of future Fe-based BMGs is to obtain the alloys with combination of large glass-forming ability (GFA) and excellent compressive ductility. Kui et al. observed that the GFA can be improved by fluxing the $Pd_{40}Ni_{40}P_{20}$ alloy in B_2O_3 [11]. Exploiting this principle, the $Pd_{40}Ni_{20}Cu_{20}P_{20}$ glassy alloy was prepared in a bulk form with a diameter up to 80 mm [12]. Meanwhile, it is important to note that most BMGs featuring the best mechanical

properties have been prepared by fluxing. Thereby, ductile $Pt_{57.7}Cu_{14.7}Ni_{5.3}P_{22.5}$ [13] and "liquid-like" $Pt_{74.7}Cu_{1.5}Ag_{0.3}P_{18}B_4Si_{1.5}$ [14] BMGs can sustain compressive loadings to failure strains exceeding 20%. Similarly, damage tolerance was also attained for a fluxed Pd-rich composition [15], and this BMG exhibits high strength along with a fracture toughness of 200 MPa·$m^{1/2}$, which is even higher than that of conventional structural metals. Recently, some results indicated that Fe-based BMGs subjected to flux treatment exhibit a promising combination of higher critical thicknesses and improved mechanical properties [16–20]. Moreover, the soft magnetic properties [21] and magnetocaloric effect [22] of fluxing Fe-based BMGs were also enhanced. It has been demonstrated that fluxing can significantly promote the purification effects [16,23]. However, further in-depth investigations of the purification mechanism still need to be pursued. Shen et al. [24,25] postulated that the GFA of the fluxed alloys is related to the amount of influencing oxygen. Chen et al. [26] revealed that fluxing induced improvement of GFA and ductility must be attributed to phase transformations and structural change, respectively. Granata et al. [27,28] proposed that the improved ductility of fluxed BMGs is induced by the purification effects. These debates indicate that a physical understanding of the mechanisms affecting this fluxing is still unsettled. Therefore, it is important to improve our understanding of the mechanisms of fluxing effects in Fe-based BMGs.

In this work, we report the effects of fluxing on $Fe_{50}Ni_{30}P_{13}C_7$ BMGs, and demonstrate that the general assumption based on the reduction of heterogeneous nucleation does not reflect the complete picture for understanding the mechanisms affecting this fluxing. By atom probe tomography (APT) analysis, we found that the employed oxide fluxing agent results in significant incorporation of boron in the alloy. The higher/improved GFA and more densely packed microstructure of the fluxed alloys are induced by the componential modification. This work is helpful for designing new BMGs with combination of high critical thicknesses and improved mechanical properties by improving the fluxing agents.

2. Experimental

$Fe_{50}Ni_{30}P_{13}C_{7-x}B_x$ (x = 0, 1 and 2) (at. %) master alloys were prepared by torch-melting a mixture of pure Fe powders (99.90 mass %), Ni powders (99.99 mass %), graphite powders (99.95 mass %), Fe_3P pieces (99.50 mass %) and pure B (99.50 mass %) crystals under a high-purity argon atmosphere. Four different modifications of $Fe_{50}Ni_{30}P_{13}C_7$ samples were performed and labeled as follows: unfluxed rod, unfluxed ribbon, fluxed rod and fluxed ribbon. For unfluxed samples, the $Fe_{50}Ni_{30}P_{13}C_7$ glassy rods and ribbons were prepared by water quenching [22,29] and the single-roller melt spinning method using the master alloys, respectively. For fluxed samples, the alloy ingots were fluxed in a fluxing agent composed of B_2O_3 and CaO with a mass ratio of 3:1 at 1500 K for several hours under a vacuum of ~ 10 Pa. After flux treatment, the rods and ribbons were prepared by water quenching and single-roller melt spinning methods, respectively. Moreover, unfluxed $Fe_{50}Ni_{30}P_{13}C_{7-x}B_x$ (x = 0, 1 and 2) samples were also prepared by water quenching and single-roller melt spinning methods, respectively.

The nature of glassy samples was ascertained by D8 Advance X-ray diffraction (XRD) with Cu Kα radiation, NETZSCH DSC-404 differential scanning calorimetry (DSC) with a heating rate of 0.67 K/s, and high-resolution transmission electron microscopy (HRTEM) using a Tecnai F20 microscope. Crystallization treatment was carried out by annealing the as-quenched amorphous specimens at 773 K for 10 min under vacuum followed by water quenching. Microstructure of crystalline samples was examined by XRD. Needle-shaped specimens for atom probe tomography (APT) were fabricated by standard two steps electro-polishing. The standing voltage on the apex of the specimen was varied automatically in order to maintain an evaporation rate of 1 ion in every 100 pulses. The APT analysis was performed in a Cameca Instruments
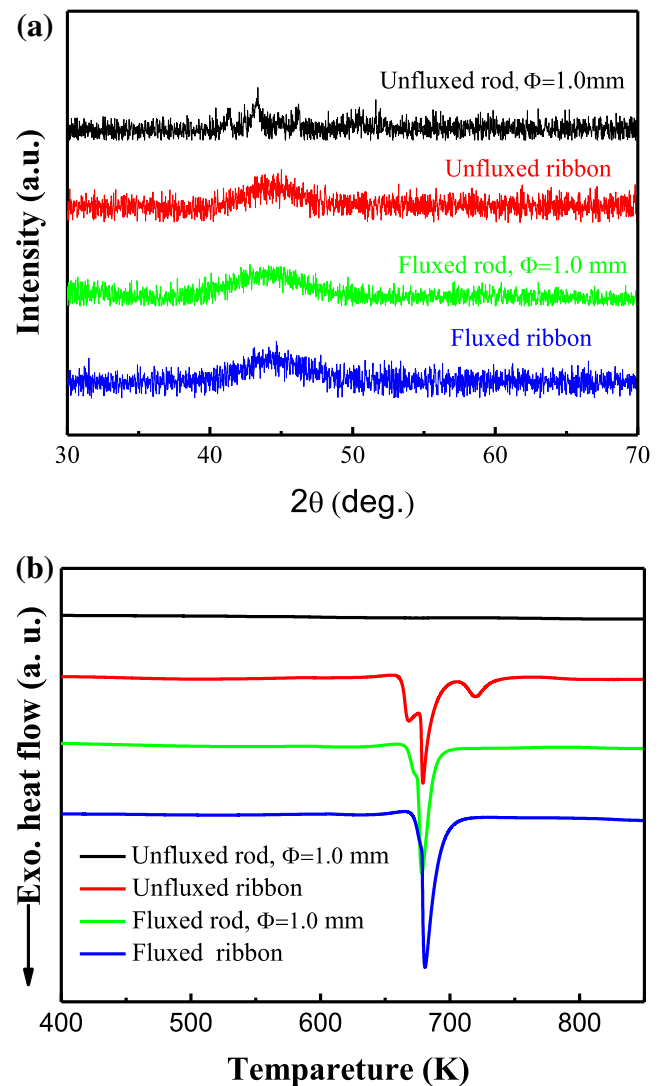
Fig. 1. (a) XRD spectra illustrating the glass-forming ability of the differently processed $Fe_{50}Ni_{30}P_{13}C_7$ samples. (b) DSC curves of the differently processed $Fe_{50}Ni_{30}P_{13}C_7$ samples (heating rate 0.67 K/s).
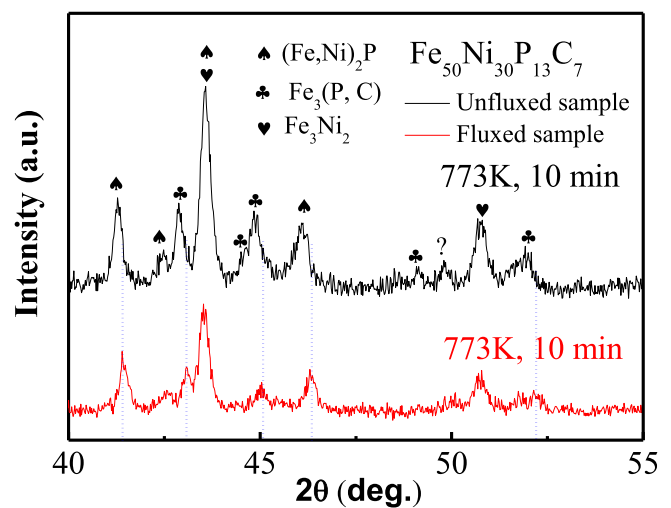
Fig. 2. XRD patterns of the fluxed and unfluxed $Fe_{50}Ni_{30}P_{13}C_7$ glassy ribbons annealed at 773 K for 10 min.
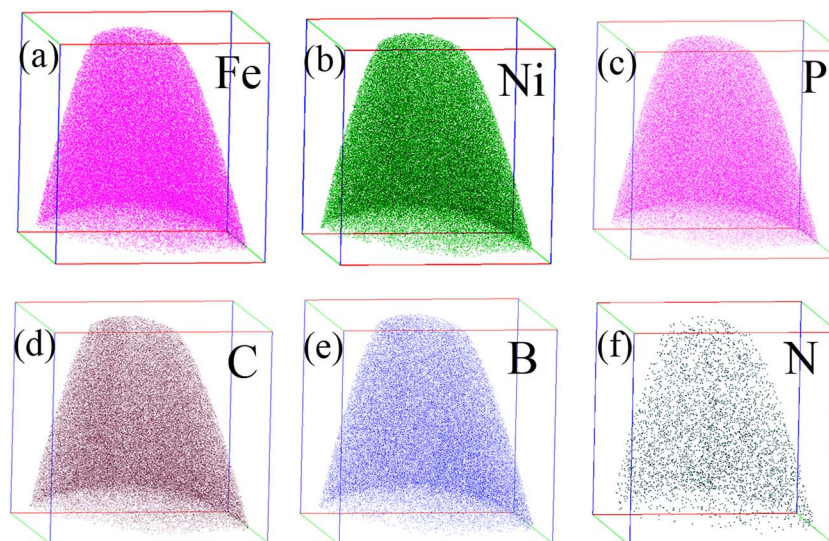
Fig. 3. The 68 × 68 × 69 nm³ section of corresponding elemental concentration profile for fluxed Fe₅₀Ni₃₀P₁₃C₇ glassy rod. The corresponding atom map for (a) the Fe distribution, (b) the Ni distribution, (c) the P distribution, (d) the C distribution, (e) the B distribution, and (f) the N distribution.

LEAP 4000× HR in either voltage or laser (pulse energy: 60 pJ, λ = 365 nm, 200 kHz pulse repetition rate) modes, the specimen was kept at a temperature of 50 K.

The specimens for compression test were cut out from the glassy rods, and each end was polished to make it parallel to each other prior to the compression test. The mechanical behavior of at least 5 glassy samples with a diameter of 1.0 mm and an aspect ratio of 2:1 was examined under uniaxial compression using an Instron testing machine at room temperature, and the strain rate was $5 \times 10^{-4} \text{ s}^{-1}$.

3. Results and discussion

Fig. 1 shows the XRD spectra and DSC curves illustrating the GFA of the differently processed Fe₅₀Ni₃₀P₁₃C₇ samples. From Fig. 1(a), only broad peaks, without crystalline diffraction evidence, can be seen for the ribbons and fluxed rods, while the unfluxed rod specimen with diameter of 1.0 mm shows crystalline diffraction peaks. Fig. 1(b) shows the DSC curves of the differently processed Fe₅₀Ni₃₀P₁₃C₇ samples. It can be seen that the thermal characteristics of unfluxed rod and unfluxed ribbon are completely different. These results suggest that the unfluxed bulk sample is not amorphous structure. Meanwhile, there is no obvious difference in exothermic peaks between the fluxed rod and ribbon. The crystallization enthalpy for the glassy rod was similar to that of glassy ribbon within the experimental error. The XRD and DSC results shown in Fig. 1 are complementary, indicating the fully amorphous structure of the fluxed cylinder rods. Apparently, all these results show that the fluxed Fe₅₀Ni₃₀P₁₃C₇ glassy alloys can be easily produced in bulk form with a diameter exceeding 1.0 mm, confirming that this alloy possesses large GFA. Furthermore, it is worthwhile to mention that the exothermic peaks strongly depend on the process conditions; the differently processed ribbons exhibit different shapes of exothermic peaks. The exothermic peaks are important material

characteristics which are sensitive to the alloy composition [26,30], indicating the fluxing agent may induce componential modification in Fe₅₀Ni₃₀P₁₃C₇ BMGs.

Fig. 2 shows the XRD patterns of crystalline phases of the unfluxed and fluxed Fe₅₀Ni₃₀P₁₃C₇ glassy ribbons annealed at 773 K for 10 min. Some sharp diffraction peaks can be observed, and the corresponding crystalline phases can be identified as (Fe, Ni)₂P, Fe₃(P, C), and Fe₃Ni₂ phases. Interestingly, it can be found that some diffraction peaks identified as (Fe, Ni)₂P and Fe₃(P, C) phases in the XRD pattern of the fluxed-treated glassy ribbon are obviously shifted to higher wave vector. According to the Bragg equation: $2r_1\sin\theta = \lambda$, the position of an X-ray halo maximum is directly related to the average radius of the first coordination shell r_1, the X-ray wave length λ, and the scatter angle corresponding to the halo maximum 2θ. The shifts of diffraction peaks may indicate the changes of configuration coordination and topological rearrangements of atoms by fluxing. In other words, the crystalline phases in fluxed sample display a more densely packed microstructure with a smaller mean atomic distance and lager coordination number.

In order to determine the factors underlying this GFA increasing, thermal characteristics changing and more densely packed microstructure of samples after fluxing, the APT analysis was conducted. The 68 × 68 × 69 nm³ section of an atom map and a corresponding elemental concentration profile of fluxed Fe₅₀Ni₃₀P₁₃C₇ glassy rod are shown in Fig. 3 and Table 1, separately. Based on the APT data, no evidence of phase separation is observed, and all the elements are homogenously distributed without any chemical segregation. It can be found that the fluxed Fe₅₀Ni₃₀P₁₃C₇ glassy rod exhibits lower content of C and P contents than its nominal composition, especially C. Surprisingly, some unexpected elements such as B and N appear in the atom map of Fe₅₀Ni₃₀P₁₃C₇ glassy rod. The negligible N atoms in the Fe-based MGs were mainly attributed to the crystalline Fe-base raw materials (the N element in interstitial sites in a b.c.c. material) [31]. This work is important to point out that fluxing has induced B addition in Fe₅₀Ni₃₀P₁₃C₇ metallic glasses.

According to metallurgical physical chemistry, Fe-rich melts can dissolve large amounts of oxygen [32]. Therefore, the following reactions in the fluxing process may take place concerning B₂O₃, CaO, C, P and FeO [33–35]:

$$B_2O_3 + 3C = 2B + 3CO \tag{1}$$

$$FeO + CO = Fe + CO_2 \tag{2}$$

$$FeO + C = Fe + CO_2 \tag{3}$$

Table 1
Elemental concentration in the fluxed Fe₅₀Ni₃₀P₁₃C₇ glassy rod.

Elements	Atomic fraction (%)	Atomic fraction (sigma)
P	12	1.9×10^{-04}
Fe	50	4.6×10^{-04}
Ni	34	3.6×10^{-04}
B	1	6.2×10^{-05}
C	3	9.1×10^{-05}
N	–	1.7×10^{-05}
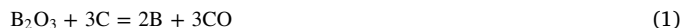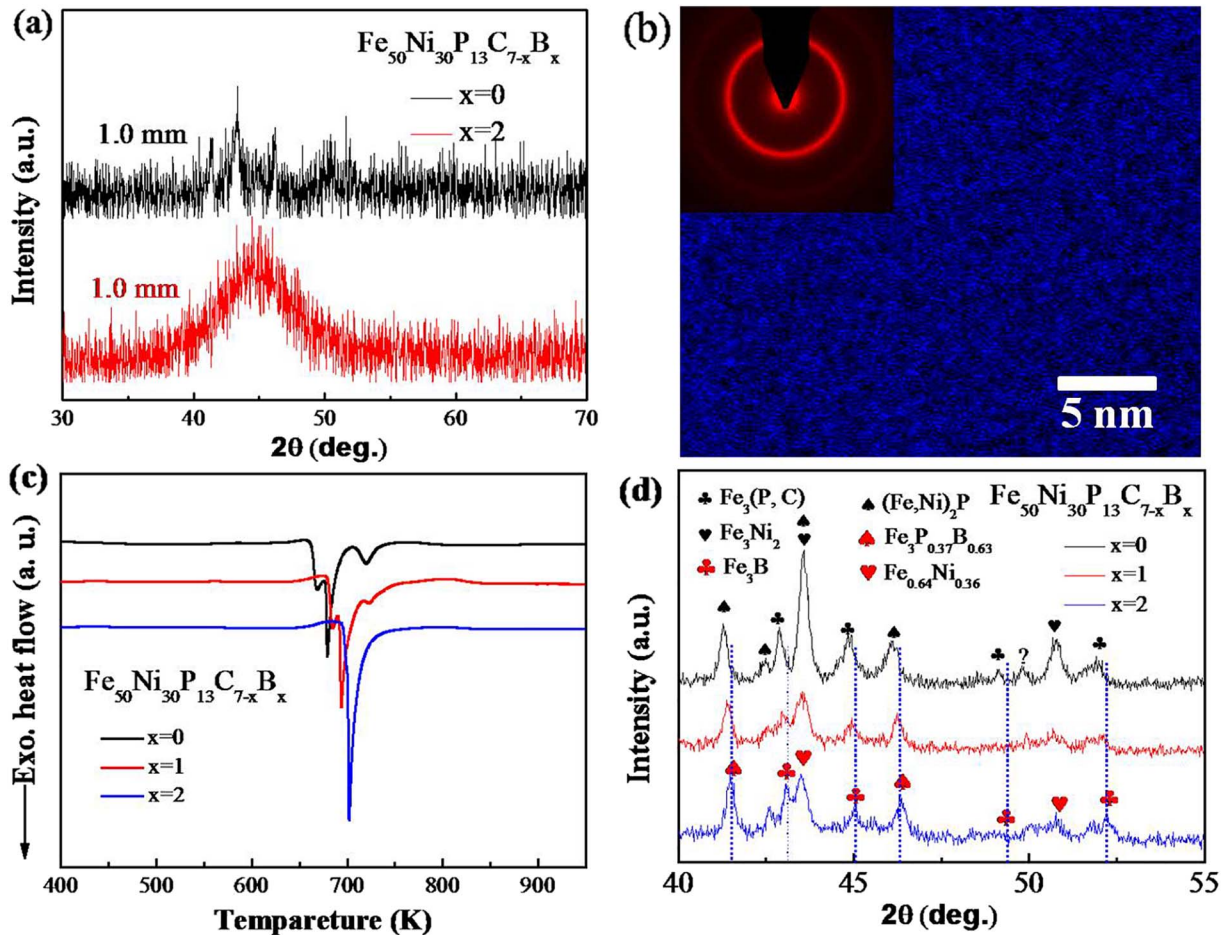
Fig. 4. (a) XRD patterns of 1.0 mm unfluxed $Fe_{50}Ni_{30}P_{13}C_7$ rods compared with 1.0 mm unfluxed $Fe_{50}Ni_{30}P_{13}C_5B_2$ rods. (b) HRTEM image of the $Fe_{50}Ni_{30}P_{13}C_5B_2$ glassy rod. The inset is the related SAED pattern. (c) DSC plots of unfluxed $Fe_{50}Ni_{30}P_{13}C_{7-x}B_x$ (x = 0, 1, 2) glassy specimens. (d) XRD patterns of the $Fe_{50}Ni_{30}P_{13}C_{7-x}B_x$ (x = 0, 1, 2) glassy specimens annealed at 773 K for 10 min.

Table 2
Thermal stability data of glassy specimens: the glass transition temperature T_g, crystallization temperature T_x and supercooled liquid region ΔT_x.

Samples			T_g (K)	T_x (K)	ΔT_x (K)
$Fe_{50}Ni_{30}P_{13}C_7$	Fluxed ribbons		642	669	27
	Fluxed rods		642	666	24
$Fe_{50}Ni_{30}P_{13}C_{7-x}B_x$	Ribbons	x = 0	642	662	20
		x = 1	650	679	29
		x = 2	652	690	38

$$2P + 5FeO + 4CaO = 4CaO·P_2O_5 + 5Fe \qquad (4)$$
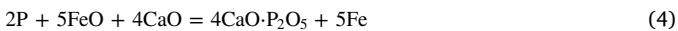
Generally, reaction (1) only occurs spontaneous above 2000 degrees Celsius. Interestingly, the CaO can promote the reaction that can occur during fluxing process [35], which results in incorporation of B into the alloy during the fluxing. In order to eliminate the residual air bubbles, the fluxing agent composed of B_2O_3 and CaO has been heated above 1500 K more than 10 min under a vacuum of ∼ 10 Pa before the metal is added to flux. In spite of this, the bubbling has also been observed on the interface between fluxing agents and melts (see Supplementary movie). It is confirmed that the CO and/or CO_2 has been formed. The CO, C and P are capable of reacting with FeO and also of binding the dissolved oxygen to form CO_2 and Calcium orthophosphate which are soluble in the quartz tube and fluxing agent, respectively. Therefore, both C and P contents have decreased and this much more than by the quantity of the B incorporation. It is worth mentioning that the oxides from reaction inside the melt can be transferred to the surface by moving the solidification front where they are trapped along with

surface impurities. From a chemical perspective, boron oxide is capable of reacting with other oxides and also of binding the dissolved oxygen to form metaborates which are soluble in the fluxing agents [27]. Thus, there is a rare existence of oxygen atoms in the fluxed glassy samples, although these elements (P, C and B) have reacted with oxygen.

Fig. 4(a) shows the XRD patterns of unfluxed $Fe_{50}Ni_{30}P_{13}C_7$ alloys compared with unfluxed $Fe_{50}Ni_{30}P_{13}C_5B_2$ alloys with 1.0 mm in diameter. It can be seen that the XRD pattern displays broad diffraction maxima, which is the characteristic of glassy structure. Meanwhile, the HRTEM image of $Fe_{50}Ni_{30}P_{13}C_5B_2$ rod and their corresponding selected area electron diffraction (SAED) pattern are shown in Fig. 4(b). No crystalline phase appears in the HRTEM, and the SAED pattern consists of a single diffraction halo without sharp diffraction rings. The thermal properties, i.e. glass transition temperature T_g, crystallization temperature T_x and the resulting supercooled liquid region ΔT_x (summarized in Table 2), were analyzed by means of DSC for all processes in Fig. 1(b) and Fig. 4(c). The fluxed $Fe_{50}Ni_{30}P_{13}C_7$ ribbon features a T_g of 642 K and a T_x of 669 K, whereas the fluxed rod displays a T_g of 642 K and a T_x of 666 K. Apparently the thermal characteristics depend strongly on the applied cooling rate during preparation. Previous results indicated that T_g and T_x increased with increasing the metalloids (P and C) content in Fe-P-C glassy systems [36]. From above analysis, besides B alloying, the C and P contents were also released in $Fe_{50}Ni_{30}P_{13}C_7$ glassy samples during the fluxing. Thus, the unfluxed $Fe_{50}Ni_{30}P_{13}C_{7-x}B_x$ (x = 1 and 2) ribbons exhibit higher glass transition temperatures and crystallization temperatures than the fluxed $Fe_{50}Ni_{30}P_{13}C_7$ ribbons. Moreover, the DSC investigations demonstrate that the ΔT_x progressively increase with B content from 20 K to 38 K for unfluxed $Fe_{50}Ni_{30}P_{13}C_{7-x}B_x$
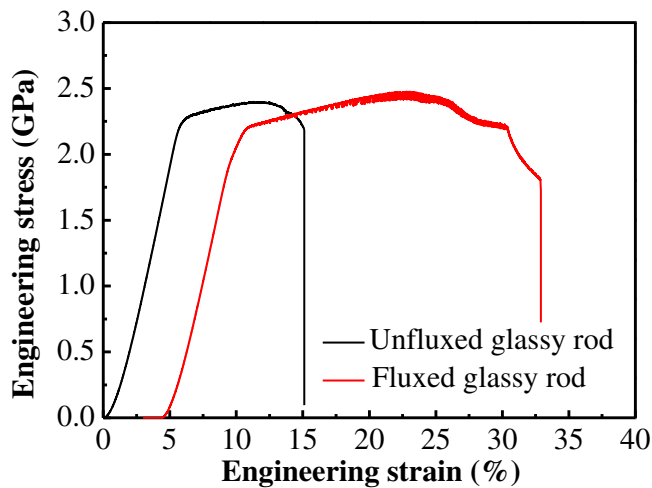
Fig. 5. Compression curves of the fluxed and unfluxed glassy rods measured at a strain rate of 5×10^{-4} for rods of 1 mm diameter.

(x = 0, 1, 2) glassy ribbons. Hence, in accordance with the Turnbull criterion [37], the GFA of $Fe_{50}Ni_{30}P_{13}C_5B_2$ is larger than that of unfluxed $Fe_{50}Ni_{30}P_{13}C_7$ alloy. This result further confirms the fact that proper B additions can enhance the critical casting thickness of Fe-based amorphous alloys [38]. Furthermore, we find that the shape of crystallization peaks is practically sensitive to the B content. With the increasing B content, crystallization peaks changed from three peaks of $Fe_{50}Ni_{30}P_{13}C_7$ to the only one peak of $Fe_{50}Ni_{30}P_{13}C_5B_2$ alloy and the T_g and T_x increased with increasing the B content, as displayed in Fig. 4(c). It is well known that the T_g of fluxed samples is notably shifted to lower temperatures as compared to the unfluxed case [27]. Hence, here the compositional changes lead to no change in T_g of fluxed $Fe_{50}Ni_{30}P_{13}C_7$ ribbon and unfluxed $Fe_{50}Ni_{30}P_{13}C_7$ ribbon. With a similar trend observed in Fig. 1(b), these data further confirm that fluxing induces B addition in $Fe_{50}Ni_{30}P_{13}C_7$ metallic glasses. It is found that the amount of P and C in fluxed alloys is lower than that of their nominal composition. Therefore, the fluxing induced modified composition must be attributed to the more densely packed microstructure with a smaller mean atomic distance and lager coordination number of $(Fe, Ni)_2P$ and $Fe_3(P, C)$ phases, as displayed in Fig. 2. The atomic sizes of P (0.108 nm) and C (0.091 nm) are larger than that of B (0.086 nm) and N (0.075 nm) [39], respectively. Compared with $Fe_{50}Ni_{30}P_{13}C_{7-x}B_x$ (x = 1 and 2), the master alloy of $Fe_{50}Ni_{30}P_{13}C_7$ does not contain B element. Thus, it can be expected that some diffraction peaks in the XRD pattern of $Fe_{50}Ni_{30}P_{13}C_{7-x}B_x$ specimens shift to higher wave vector with the increasing B content, which can be confirmed in Fig. 4(d). The crystalline phases in XRD patterns of $Fe_{50}Ni_{30}P_{13}C_{7-x}B_x$ (x = 1 and 2) glassy ribbons annealed at 773 K for 10 min can be identified as $Fe_3P_{0.37}B_{0.63}$, Fe_3B, and $Fe_{0.64}Ni_{0.36}$ phases. Apparently, the $Fe_3P_{0.37}B_{0.63}$ and Fe_3B phases display more densely packed microstructure with smaller mean atomic distance and lager coordination number than that of $(Fe, Ni)_2P$ and $Fe_3(P, C)$ phases, respectively.

Up to now, boron oxide has been the standard fluxing agent for Fe-, Pd-, Pt-based BMGs [14,40,41], as introduced to the community by Kui et al. in 1984 [11]. In general, glass-forming compositions subjected to boron oxide fluxing feature the best combination of high fracture toughness and compressive ductility [13], and fluxed BMGs also exhibit improved GFA [42] and enhanced thermal stability [41]. Especially, the fluxing-induced improvement of ductility was found for various alloys prepared [14,15,27,41,43]. As previous researches, the mechanical properties were also performed for fluxed and unfluxed glassy rods. The plastic strain of fluxed glassy rods reaches values of ~20% (comparable to reported values in ref. [19]), whereas the plastic strain

is only ~10% for the unfluxed sample, as shown in Fig. 5. The substantial enhancement of compressive plasticity can be correlated with lower contents of oxygen [27] and larger volume of shear transformation zones [41]. Here, fluxing induced B alloying in Fe-based BMGs was observed firstly in this study. Generally speaking, proper addition of B is an effective approach to improving the GFA and thermal stability in Fe- [44], Ni- [45] and Co-based BMGs [46]. But there are exceptions that the minor B alloying degrades the achievable GFA of Pd-Si-Cu BMGs due to an increase in the liquids temperature [25]. In principle, the performances of BMGs are strongly affected by compositional modifications and thermal history. Therefore, the development of further fluxing agents is crucial for enhancement of the key properties of BMGs.

4. Conclusion

In this work, the effects of fluxing on $Fe_{50}Ni_{30}P_{13}C_7$ samples were studied using atom probe tomography. It is shown that the reduction of heterogeneous nucleation does not reflect the complete picture for understanding the mechanisms affecting fluxing treatment. The GFA and thermal characteristics are strongly linked with different preparation processes, e.g. fluxing and unfluxing. It is demonstrated that fluxing leads to compositional modification and influences the GFA and local microstructure difference of $Fe_{50}Ni_{30}P_{13}C_7$ BMGs. A large amount of carbon in the alloy is substituted by boron. Such an understanding is of great importance to adequately process glass-forming liquids, in order to achieve optimized metallic glassy parts with enhanced thicknesses and improved mechanical properties.

Supplementary data to this article can be found online at http://dx.doi.org/10.1016/j.matdes.2017.05.020.

Author contributions

W. Y., C. W., H. L., B. S., and Q. L conceived and designed the research and analysis. J. Z., and L. X., provided the DSC data. H. L. analyzed atom probe tomography experimental data. W. Y., H. L., Q. W., and A. I. co-wrote the paper. All authors discussed the results and revised the manuscript.

References

[1] C. Suryanarayana, A. Inoue, Iron-based bulk metallic glasses, Int. Mater. Rev. 58 (2013) 131–166.

[2] Y. Geng, Y. Wang, Z. Wang, J. Qiang, H. Wang, C. Dong, O. Tegus, Formation and structure-property correlation of new bulk Fe-B-Si-Hf metallic glasses, Mater. Des. 106 (2016) 69–73.

[3] J. Li, L. Yang, H. Ma, K. Jiang, C. Chang, J.-Q. Wang, Z. Song, X. Wang, R.-W. Li, Improved corrosion resistance of novel Fe-based amorphous alloys, Mater. Des. 95 (2016) 225–230.

[4] Y. Zhou, G. Ma, H. Wang, G. Li, S. Chen, H. Wang, M. Liu, Fabrication and characterization of supersonic plasma sprayed Fe-based amorphous metallic coatings, Mater. Des. 110 (2016) 332–339.

[5] S.F. Guo, F.S. Pan, H.J. Zhang, D.F. Zhang, J.F. Wang, J. Miao, C. Su, C. Zhang, Fe-based amorphous coating for corrosion protection of magnesium alloy, Mater. Des. 108 (2016) 624–631.

[6] Z.P. Lu, C.T. Liu, J.R. Thompson, W.D. Porter, Structural amorphous steels, Phys. Rev. Lett. 92 (2004) 245503.

[7] K.F. Yao, F. Ruan, Y.Q. Yang, N. Chen, Superductile bulk metallic glass, Appl. Phys. Lett. 88 (2006) 122106.

[8] J. Shen, Q.J. Chen, J.F. Sun, H.B. Fan, G. Wang, Exceptionally high glass-forming

ability of an FeCoCrMoCBY alloy, Appl. Phys. Lett. 86 (2005) 151907.

[9] H.Y. Jung, S.J. Choi, K.G. Prashanth, M. Stoica, S. Scudino, S. Yi, U. Kühn, D.H. Kim, K.B. Kim, J. Eckert, Fabrication of Fe-based bulk metallic glass by selective laser melting: a parameter study, Mater. Des. 86 (2015) 703–708.

[10] G.N. Yang, Y. Shao, K.F. Yao, The material-dependence of plasticity in metallic glasses: an origin from shear band thermology, Mater. Des. 96 (2016) 189–194.

[11] H.W. Kui, A.L. Greer, D. Turnbull, Formation of bulk metallic glass by fluxing, Appl. Phys. Lett. 45 (1984) 615.

[12] N. Nishiyama, K. Takenaka, H. Miura, N. Saidoh, Y. Zeng, A. Inoue, The world's biggest glassy alloy ever made, Intermetallics 30 (2012) 19–24.

[13] J. Schroers, W.L. Johnson, Ductile bulk metallic glass, Phys. Rev. Lett. 93 (2004) 255506.

[14] M.D. Demetriou, M. Floyd, C. Crewdson, J.P. Schramm, G. Garrett, W.L. Johnson, Liquid-like platinum-rich glasses, Scr. Mater. 65 (2011) 799–802.

[15] M.D. Demetriou, M.E. Launey, G. Garrett, J.P. Schramm, D.C. Hofmann, W.L. Johnson, et al., A damage-tolerant glass, Nat. Mater. 10 (2011) 123–128.

[16] M. Stoica, K. Hajlaoui, A. Lemoulec, A.R. Yavari, New ternary Fe-based bulk metallic glass with high boron content, Philos. Mag. Lett. 86 (2006) 267–275.

[17] X.H. Ma, X.H. Yang, Q. Li, S.F. Guo, Quaternary magnetic FeNiPC bulk metallic glasses with large plasticity, J. Alloys Compd. 577 (2013) 345–350.

[18] K.F. Yao, C.Q. Zhang, Fe-based bulk metallic glass with high plasticity, Appl. Phys. Lett. 90 (2007) 061901.

[19] W. Yang, H. Liu, Y. Zhao, A. Inoue, K. Jiang, J. Huo, H. Ling, Q. Li, B. Shen, Mechanical properties and structural features of novel Fe-based bulk metallic glasses with unprecedented plasticity, Sci. Rep. 4 (2014) 6233.

[20] W. Yang, B. Sun, Y. Zhao, Q. Li, L. Hou, N. Luo, C. Dun, C. Zhao, Z. Ma, H. Liu, B. Shen, Non-repeatability of large plasticity for Fe-based bulk metallic glasses, J. Alloys Compd. 676 (2016) 209–214.

[21] T. Bitoh, D. Shibata, Constant permeability of $(Fe_{0.75}B_{0.20}Si_{0.05})_{96}Nb_4$ bulk metallic glass prepared by B_2O_3 flux melting and Cu-mold casting, J. Appl. Phys. 105 (2009) 07A312.

[22] W. Yang, J. Huo, H. Liu, J. Li, L. Song, Q. Li, L. Xue, B. Shen, A. Inoue, Extraordinary magnetocaloric effect of Fe-based bulk glassy rods by combining fluxing treatment and J-quenching technique, J. Alloys Compd. 684 (2016) 29–33.

[23] L. Sun, Q. Wu, Y. Xu, W. Wang, Study on solidification behaviour of $Pd_{40}Ni_{40}P_{20}$ alloy by fluxing method, Physica B 240 (1997) 205–210.

[24] T.D. Shen, R.B. Schwarz, Bulk ferromagnetic glasses in the Fe-Ni-P-B system, Acta Mater. 49 (2001) 837–847.

[25] T. Shen, R. Schwarz, Bulk ferromagnetic glasses prepared by flux melting and water quenching, Appl. Phys. Lett. 75 (1999) 49–51.

[26] N. Chen, L. Gu, G.Q. Xie, D.V. Louzguine-Luzgin, A.R. Yavari, G. Vaughan, S.D. Imhoff, J.H. Perepezko, T. Abe, A. Inoue, Flux-induced structural modification and phase transformations in a $Pd_{40}Ni_{40}Si_4P_{16}$ bulk-glassy alloy, Acta Mater. 58 (2010) 5886–5897.

[27] D. Granata, E. Fischer, V. Wessels, J.F. Löffler, Fluxing of Pd-Si-Cu bulk metallic

glass and the role of cooling rate and purification, Acta Mater. 71 (2014) 145–152.

[28] D. Granata, E. Fischer, V. Wessels, J. Löffler, The detrimental effect of flux-induced boron alloying in Pd-Si-Cu bulk metallic glasses, Appl. Phys. Lett. 106 (2015) 011902.

[29] Q. Li, Formation of ferromagnetic bulk amorphous $Fe_{40}Ni_{40}P_{14}B_6$ alloys, Mater. Lett. 60 (2006) 3113–3117.

[30] W. Yang, H. Liu, X. Fan, L. Xue, C. Dun, B. Shen, Enhanced glass forming ability of Fe-based amorphous alloys with minor Cu addition, J. Non-Cryst. Solids 419 (2015) 65–68.

[31] J.M. Pelletier, B. Van de Moortèle, I.R. Lu, Viscoelasticity and viscosity of Pd-Ni-Cu-P bulk metallic glasses, Mater. Sci. Eng. A 336 (2002) 190–195.

[32] H.A.C.J. Wriedt, Oxygen in liquid iron-nickel alloys, JOM 8 (1956) 1195–1199.

[33] D.G. Zhao, S.H. Wang, P. Zhao, Thermodynamic of boron oxide reducing with carbothermic method, J Iron Steel Res. 24 (2012) 19–22.

[34] Y.K.K. Shirota, K. Klein, H.-J. Engell, D. Janke, Phosphate capacity of FeO-Fe$_2$O$_3$-CaO-P$_2$O$_5$ and FeO-Fe$_2$O$_3$-CaO-CaF$_2$-P$_2$O$_5$ slags by levitation melting, J. Iron Steel Inst. Jpn. 25 (1985) 1132–1140.

[35] J.L. Dingguo Zhao, Shuhuan Wang, Dynamics research of direct alloying smelting boron steel, Foundry Technol. 35 (2014) 2339–2342.

[36] T.D. Shen, B.R. Sun, S.W. Xin, Effects of metalloids on the thermal stability and glass forming ability of bulk ferromagnetic metallic glasses, J. Alloys Compd. 631 (2015) 60–66.

[37] D. Turnbull, Under what conditions can a glass be formed, Contemp. Phys. 10 (1969) 473–488.

[38] F. Luborsky, J. Becker, J. Walter, D. Martin, The Fe-BC ternary amorphous alloys, IEEE Trans. Magn. 16 (1980) 521–525.

[39] J.G. Speight, M. Graw-Hill (Ed.), Lang's Handbook of Chemistry, 2005, p. 1.151 (London).

[40] T.D. Shen, S.W. Xin, B.R. Sun, Low power loss in $Fe_{65.5}Cr_4Mo_4Ga_4P_{12}B_{5.5}C_5$ bulk metallic glasses, J. Alloys Compd. 658 (2016) 703–708.

[41] N. Chen, D. Pan, D. Louzguine-Luzgin, G. Xie, M. Chen, A. Inoue, Improved thermal stability and ductility of flux-treated $Pd_{40}Ni_{40}Si_4P_{16}$ BMG, Scr. Mater. 62 (2010) 17–20.

[42] T.D. Shen, R.B. Schwarz, Bulk ferromagnetic glasses prepared by flux melting and water quenching, Appl. Phys. Lett. 75 (1999) 49.

[43] K.-F. Yao, Y.-Q. Yang, N. Chen, Mechanical properties of Pd-Cu-Si bulk metallic glass, Intermetallics 15 (2007) 639–643.

[44] F.E. Luborsky, H.H. Liebermann, Crystallization kinetics of Fe-B amorphous alloys, Appl. Phys. Lett. 33 (1978) 233.

[45] J.H. Na, M.D. Demetriou, M. Floyd, A. Hoff, G.R. Garrett, W.L. Johnson, Compositional landscape for glass formation in metal alloys, PNAS 111 (2014) 9031–9036.

[46] C. Dun, C. Liu, B. Shen, Enhancement of plasticity in Co-Nb-B ternary bulk metallic glasses with ultrahigh strength, J. Non-Cryst. Solids 358 (2012) 3060–3064.